13.4 CAPACITANCE OF SNOWFLAKES

Paul R. Field[1]*, A. J. Heymsfield[1], A. Bansemer[1] and C. H. Twohy[2]
1. National Center for Atmospheric Research , Boulder, Colorado
2. Oregon State University, Corvallis, Oregon

1. Introduction

Ice crystal and snow growth rates are commonly computed using growth equations developed using the electrostatic analogy: the distribution of water vapor density around an ice crystal in steady state satisfies Laplace's equation just as the electrostatic potential around a conductor does. For the electrostatic case Gauss' law states that the current flowing through a surface that encloses a volume containing a conductor is proportional to the charge contained within the volume and hence located on the conductor. For the vapor case Gauss' law says that the flux of vapor density through a surface will be proportional to the rate of change of mass of the ice crystal. The proportionality constants in the electrostatic case include a capacitance. Hence, the use of the term capacitance in referring to the ice crystal shape factor that controls how efficiently the ice crystal acts as a source or sink of water vapor.

McDonald (1963) and Podzimek (1966) exploited the electrostatic analogy to generate estimates of the capacitance of ice crystals by measuring the capacitances of metal replicas, finding good agreement with some theoretically expected results. This approach has been taken a step further by Chiruta and Wang (2003, 2005) who modeled the capacitance of multi-arm bullet rosette and hollow hexagonal column crystals by utilizing a finite element technique to solve Laplace's equation. Crystal growth rates measured by Bailey and Hallett (2004) in a static diffusion chamber suggest that theoretical estimates of capacitance for well defined objects overestimate the actual growth because the asymmetries and defects present in actual ice crystals are not taken into account. However, their results do suggest that an equivalent capacitance can be derived for ice crystals of differing habits. Deviation from the electrostatic analogy raises the possibility that growth and sublimation may not be symmetric processes and that the equivalent capacitance may vary slightly for the two processes.

For numerical weather and climate models the bulk of precipitation ice cloud will be dominated by aggregates of ice crystals (snowflakes). The time evolution of the model vapor and ice water content (IWC) fields and the frequency at which the models predict mixed-phase conditions will be strongly influenced by the capacitance chosen to represent snowflakes. It is difficult to manipulate and characterize snowflakes in the laboratory and so no value of capacitance has been proffered by experimentalists for this 'habit'. Therefore, modelers have been forced into choosing a value for capacitance to represent snow. The choice has typically been to assume a value appropriate for a disk or a sphere.

In this paper we present an estimate for the capacitance of snowflakes based on the analysis of aircraft observations made in the anvil of a large convective storm. The flight strategy followed the Lagrangian spiral descent philosophy in which the aircraft is allowed to drift with the wind as it descends at a rate close to the mass weighted fallspeed of the snowflakes. The intention of this maneuver is to repeatedly sample the same collection of ice crystals as they fall through the atmosphere allowing the observation of the evolution of the ice particle size distributions (PSDs). By carefully measuring the ice PSDs, IWC, ambient temperature, pressure and relative humidity we are able to predict the observed change in IWC from the measured environmental conditions and the PSD through the appropriate choice of capacitance.

2. Data

2.1 Lagrangian spiral descent

The data were obtained between 21:24:10 and 21:47:30 on the 26th July 2002 with the University of North Dakota Citation aircraft as part of the CRYSTAL-FACE project. The aircraft sampled the anvil part of a convective storm performing a Lagrangian spiral descent (1.5 m s^{-1}). During most of this period the air was subsaturated with respect to ice and so IWC was being reduced as the ice particles sublimated. The altitude difference between

* *Corresponding author address*: Paul R. Field NCAR, PO Box 3000, Boulder, CO 80307; e-mail: prfield@ucar.edu.

consecutive loops of the spiral was ∼200m. For subsequent analysis the loop was divided into four quadrants (subsequently referred to as regions I, II, III, IV). The regions each contain 30–35 s of flight track or 6–7 5 s averaging intervals (∼3 km flight track) arranged in discrete vertical intervals.

2.2 Particle treatment

The PSDs, using maximum particle sizes, are derived from combining data from two optical array probes: a Particle Measuring Systems 2D-C and a Stratton Park Engineering Company (SPEC) Inc. High Volume Particle Spectrometer (HVPS). Particles smaller than 100 μm were ignored due to difficulties with determining particle size and appropriate sample volume. We have not made use of data from the Forward Scattering Spectrometer Probe (FSSP) to assess the effect of particles smaller than 100 μm because of difficulties introduced by particles shattering on the housing of the probe and contaminating the FSSP signal. The 2D-C and HVPS have pixel resolutions of 30 and 200x400 μm, respectively. The 2D-C has a maximum array width of 960 μm, but it is possible to reconstruct partially imaged particles. This was done for the 2D-C, but only complete images were used in the analysis of the HVPS data. Particles rejection criteria can be found in Field et al. 2006.

2.3 Ice mass and fallspeed

It is important for the determination of the change in ice mass that the mass of the particles and terminal velocity of the particles is estimated accurately. To this end we assume a mass–dimension power law of the form $m = aD^b$ and vary the prefactor and exponent until we find a minimum rms difference between 5s estimates of IWC from the Counterflow Virtual Impactor (CVI) instrument and the IWC obtained from integrating the size distribution combined with the mass–dimension relation. The CVI provides an estimate of IWC with an associated uncertainty of 15%. The CVI ingests ice particles with sufficient inertia (equivalent to a 7μm diameter droplet at ∼110 m s^{-1}) to overcome the counterflow and measures the water content of the evaporated crystals using absorption hygrometry. The CVI inlet has a diameter of 6300 μm. It is unclear how efficiently the CVI samples particles of similar dimensions to the inlet. Using the best mass–dimension relationship suggests that ∼10% of the IWC may be found in sizes larger than 6300μm. We will use sensitivity tests to address this potential bias.

A comparison of integrated PSD data with CVI IWC suggests that a mass–dimension relationship of $m = 0.024D^{1.85}$ provides a satisfactory fit to the CVI data. For the particle fallspeed we have combined environmental parameters, particle cross-sectional area and mass with a Reynolds–Best number parametrization appropriate for aggregates described in Mitchell and Heymsfield (2005).

2.4 Relative humidity

Measurements of water vapor density were obtained with an EG&G chilled mirror and tunable diode laser (TDL) hygrometers. These measurements were combined with temperature measurements to provide an estimate of the relative humidity (RH). Comparison of the EG&G hygrometer relative humidity in liquid clouds during one of the CRYSTAL flights (9th July) indicates that the mode in a histogram of RH with respect to water was located at 98%. Similarly, for ice clouds from all flights in the CRYSTAL campaign the mode in histogram of RH with respect to ice derived from the TDL was at about 94%. The mode in the ice histogram for the EG&G was too broad to decide if it differed significantly from a value of 100%. In the following analysis we will make use of the data as published on the CRYSTAL archive, but will investigate the possibility that the measurement of RH suffers from some dry bias.

2.5 Descent profiles

Figure 1 shows mean values for various parameters for each of the four regions as a function of ambient temperature. Fig. 1a indicates that the cloud was subsaturated with respect to ice (EGG). IWC shows a decrease from 0.8 to 0.3 g m^{-3} in fig. 1b. Precipitation rate decreases from 6 to 2 mm hr^{-1} (fig. 1c), while the mass weighted fallspeed does not vary widely from 2.1 m s^{-1} (fig. 1d). The characteristic size of the PSD (defined as the ratio of the 3rd and 2nd moments of the PSD) increases from 3000 to 5000 μm (fig 1e). Concentration of particles larger than 100 μm is shown to decrease by a factor of 10 from 2×10^4 to 2×10^3 m^{-3} (fig. 1f).

Fig. 2a shows example PSDs from region I from three levels (-8, -5, -2C) and the ratio of the PSD at the lower two levels (-5, -2C) to the top level (-8C). It can be seen that while aggregation is acting to increase the concentrations of 5000-10000 μm particles between -8C and -5C, this enhancement has been reduced by the time the particles

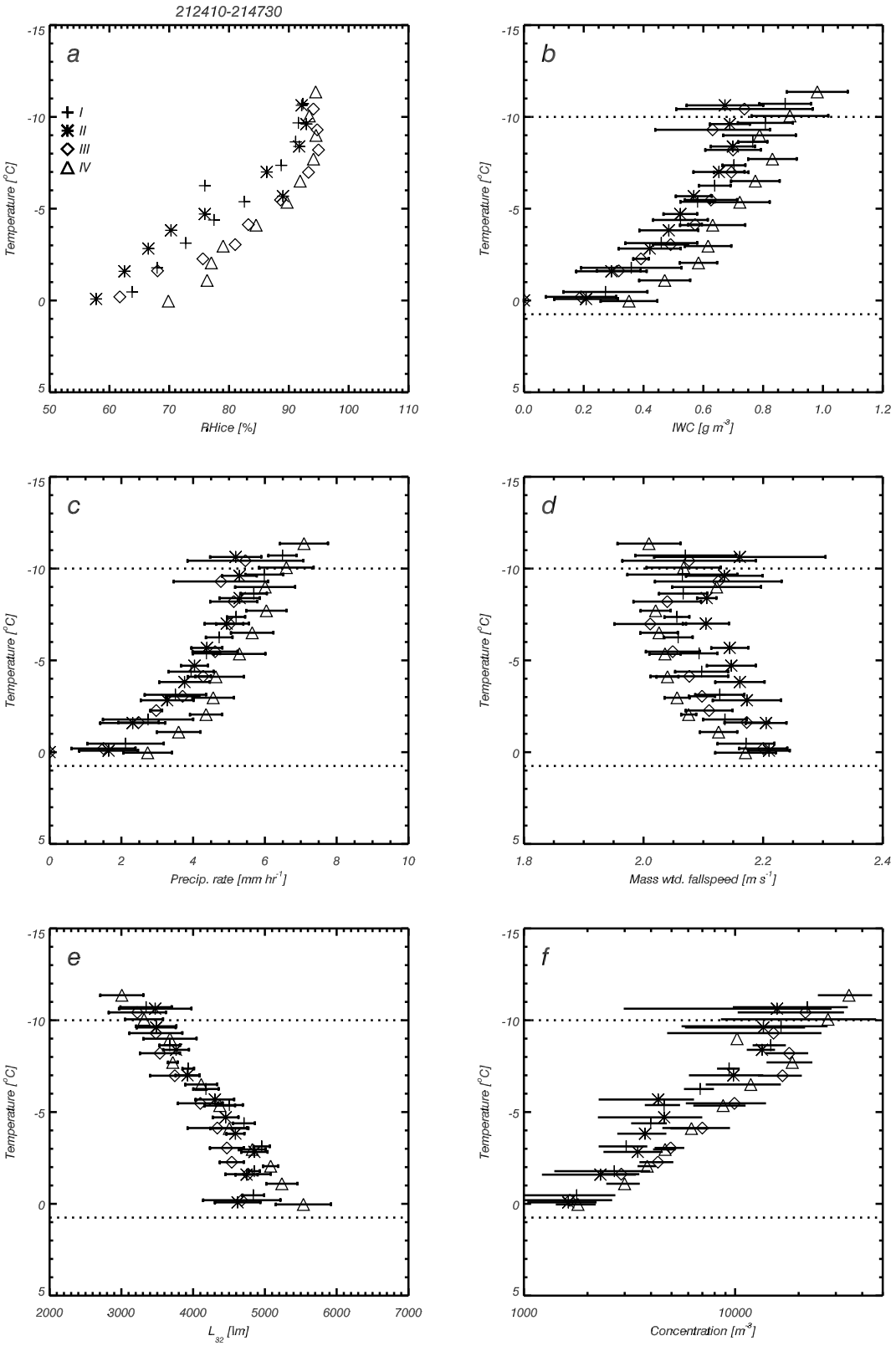

Figure 1: Average values ($\sim$3 km flight track; 30–35 s) for each region of interest as a function of temperature at which the measurement was made in the spiral. Standard deviations obtained from 6–7 5s periods along each $\sim$3 km flight track are also given as horizontal bars. The horizontal dotted lines mark the vertical extent of the sublimation zone considered in the text. a) Relative humidity with respect to ice. b) Ice water content from optical array probes. c) Precipitation rate. d) Mass weighted fall speed. e) Characteristic size. f) Concentration of particles with size $>$ 100 μm.

have reached the -2C level. The strong depletion of particles smaller than 5000μm means that the slope of the size distribution becomes shallower and the characteristic size of the distribution becomes larger. It appears that for this case the increase in characteristic size seen in fig. 1e is mainly a result of sublimation acting on the PSD.

3. Sublimation

As mentioned in the introduction, implicit in the electrostatic analogy is the assumption that diffusional growth and sublimation are symmetric processes. The equation describing the rate of mass change,dM/dt, of an ice particle through diffusional growth or sublimation is given by

$$\frac{\mathrm{d}M}{\mathrm{d}t} = 4\pi f C S_i \left(\frac{1}{\frac{L}{kT}\left(\frac{LM_w}{RT} - 1\right) + \frac{RT}{D_v M_w e_{si}}} \right) \quad (1)$$

where f is the ventilation coefficient (Pruppacher and Rasmussen, 1979), C is the capacitance or shape factor of the snowflake, S_i is the supersaturation with respect to ice obtained from the EG&G hygrometer, L is the latent heat of sublimation, M_w is the molecular weight of water, k is the conductivity of moist air, D_v is the diffusivity of water vapor, R is the universal gas constant, T is the ambient air temperature, e_{si} is the saturation vapor pressure over ice surface at temperature T. This equation along with a derivation can be found in Pruppacher and Klett (1997, Chapter 13). We have taken the values for the constants used in equation 1 from Pruppacher and Klett (1997).

We estimated the change in IWC at each level to allow comparison with the data obtained from the aircraft. We started at loop 2 (temperature = -10C) and computed the expected change in IWC between levels with

$$\Delta IWC_n = \Delta t_n \int \frac{\mathrm{d}M(D)}{\mathrm{d}t} \mathrm{d}D. \quad (2)$$

dM/dt is evaluated using midlevel values of the PSD, S_i, T, p and size dependent terminal velocities that are determined by taking the mean of adjacent levels $(n, n-1)$. Δt is obtained by dividing the difference in altitudes between the two levels by the midlevel estimate of the mass weighted fallspeed. It was found that the peak in d$M(D)$/dt is located close to the characteristic size and hence the mass weighted size too. The value of the ventilation coefficient at the peak is 6–7 throughout the spiral. A cumulative plot indicates that 80% of the change in IWC is through ice loss from particles bigger than 1000 μm, and hence dominated by the sublimation of ice aggregates or snowflakes.

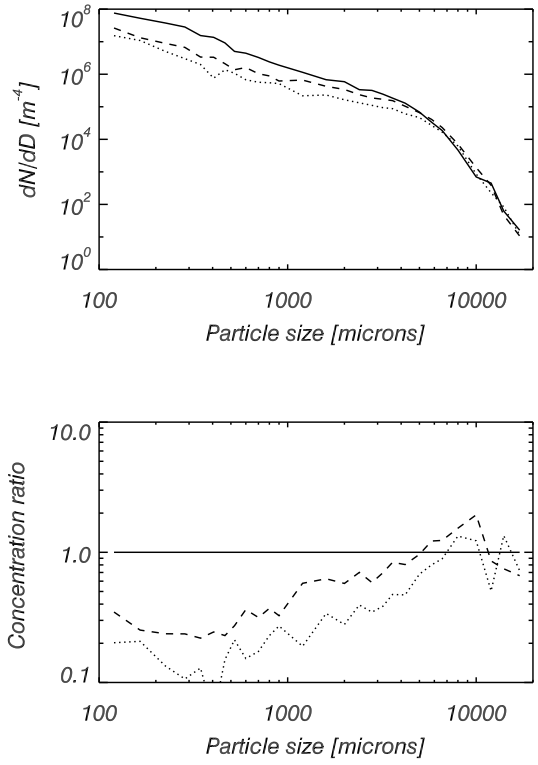

Figure 2: top) Example size distribution evolution from region I, -8C: solid, -5C: dashed, -2C: dotted. bottom) Ratio of size distribution at -5C (dashed) and -2C (dotted) to that at -8C.

We generated profiles of computed IWC for different values of capacitance and used the rms difference between the predicted and PSD estimated IWC to obtain the best estimate of capacitance in each of the four regions separately, and one value that best satisfied all the regions simultaneously. This method naturally weights points lower down in the spiral from the start position where the IWC exhibits larger deviations from the start value near the top.

Fig. 3 shows the IWC results using the control assumptions for all four regions as a function of altitude. The solid line represents the result for a capacitance of 0.23D (where D is the maximum dimension of the crystal) that produced the best agreement between the computed and observed IWC in all four regions simultaneously. The best capacitances determined from each region separately were 0.24D, 0.21D, 0.19D, 0.26D. The gray line shows the result for assuming the capacitance

appropriate for a sphere (0.5D). All regions show good agreement with the evolution in IWC predicted from the capacitance value found to best satisfy all the regions simultaneously. By referring to the gray curve it is clear to see that the assumption of capacitance appropriate for a sphere will lead to sublimation of the cloud being much more rapid. In fact, the difference would likely be more pronounced if we did not prescribe the PSD at each level and instead allowed the PSD to evolve under the action of sublimation.

4. Sensitivity tests

Bias could be introduced to the results from our selection of relationships and assumptions in the above analysis. To investigate the robustness of the result we have investigated some alternative scenarios. i) Alternately decrease and increase the estimated particle masses by 20% (this variation also generates changes in particle fallspeeds). ii) Alternately decrease and increase the estimated particle fallspeeds by 20%. iii) Alternately decrease and increase the measured relative humidity by 3%. iv) Use the relative humidity estimate from the TDL. iv) Vary the start level for the analysis by 1 and 2 levels. v) Use alternative expressions for the ventilation coefficient (Hall and Pruppacher, 1976; Thorpe and Mason, 1966).

Fig. 4 depicts the results of the sensitivity tests. The spread in minimum to maximum capacitances obtained for each region separately varies between $\sim$0.07D-0.14D. Increasing (decreasing) the particle masses, fallspeeds and ambient relative humidity leads to an increase (decrease) in the capacitance solution. Starting the analysis at one or two levels down makes a slight increase to the capacitance solution. Using the Hall and Pruppacher (1976) ventilation coefficient has little effect on the solution. Using the Thorpe and Mason (1966) ventilation coefficient results in solutions with lower values than the control.

5. Discussion and summary

An obvious limitation to this study is that it is just a single case and the results are dominated by particles with sizes between 3000–5000μm. It may be the case that capacitance will vary as a function of size: small particles exhibit their pristine habits, while larger particles are aggregates. We argue that self similarity exhibited by snowflakes means that the capacitance value obtained in this study may be applicable over a wide range of unrimed precipitation size particles. To test this assertion more observations have to be made either in the laboratory or from aircraft. In the case of the latter there is a requirement that the aircraft perform Lagrangian spiral descents at a rate commensurate with the mass weighted fallspeed, measure relative humidity to within 3%, and IWC to within 20%.

Another limitation is that the estimate of capacitance is tied to the choice of ventilation coefficient. Ji and Wang (1999) show modeling results that suggest that the ventilation coefficient will even vary with shape. Therefore the ventilation coefficient and capacitance may be deeply intertwined. The solution to this would be to collect aggregates and measure their growth rates in a laboratory setup where the effects of ventilation can be removed. Once the capacitance is known, then the ventilation coefficient for snowflakes could be determined by observing the mass change of suspended snowflakes in a moist airflow.

The Lagrangian spiral descent makes the assumption that the aircraft is following the same collection of ice crystals as they evolve. Unfortunately, the aircraft was descending slightly slower than the mass weighted fallspeed (1.5 versus 2.1 m s^{-1}). For this descent rate variation to be unimportant imposes a requirement for vertical homogeneity within the cloud to increase linearly throughout the descent to a maximum of 160m.

We would expect the mode in relative humidity with respect to water to be close to 100% for liquid clouds. In the absence of significant sustained vertical motions we would expect the mode in relative humidity with respect to ice in ice only clouds to also be centered on 100%. As noted in section 2.4 the modes of the histograms of relative humidity derived from the hygrometers and temperature data found at slightly drier relative humidities than we might expect. Therefore it is possible that the hygrometer data used has a slight dry bias. If that is the case then a realistic estimate of the capacitance for snowflakes would have a value more similar to that expected for a disk as suggested by the RH+3% sensitivity test.

One other potential source of error to note is the uncertainty in the measured size distributions. There are two ways to consider this effect. i) The Poisson counting error associated with the particle sizes that contribute most to d$M/$dt. For these sizes (3000-5000μm) the numbers of particles counted in each region over each loop was $\sim$1000 resulting in an estimated error of 3%. ii) Consider the variability within the region using the 6–7 5s periods that make up the region mean values. This is accomplished by estimating an error in the mean bias by combining the fractional stan-

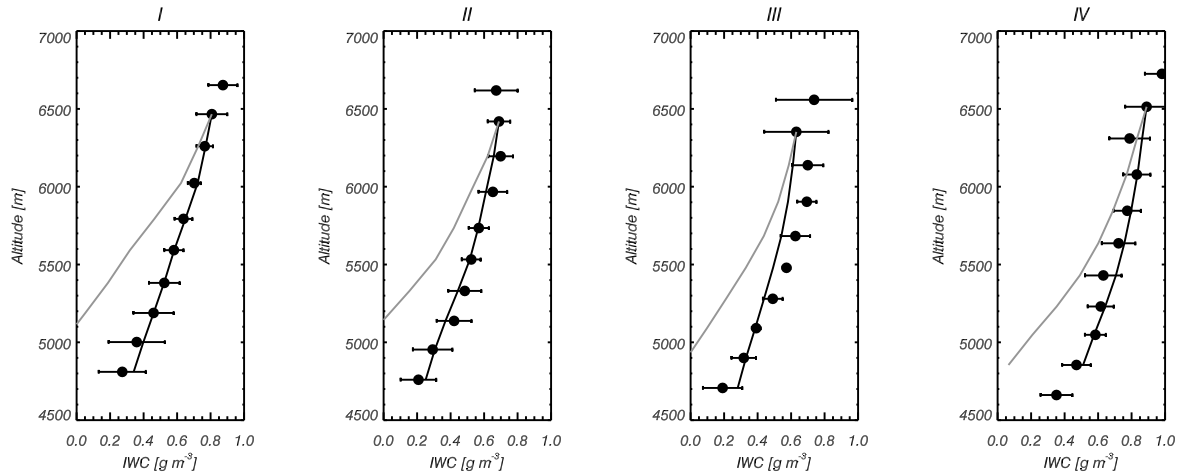

Figure 3: Measured IWC profiles (solid circles) as a function of altitude. Each point represents a mean within each of the regions over all of the loops in the spirals (30-35s average). The error bars represent the standard deviation derived from 6-7 5s averages within each region. The solid line shows the predicted profile of IWC when a capacitance for snow of 0.23D is assumed. The grey line shows the profile if the capacitance appropriate for a sphere (0.50D) is assumed.

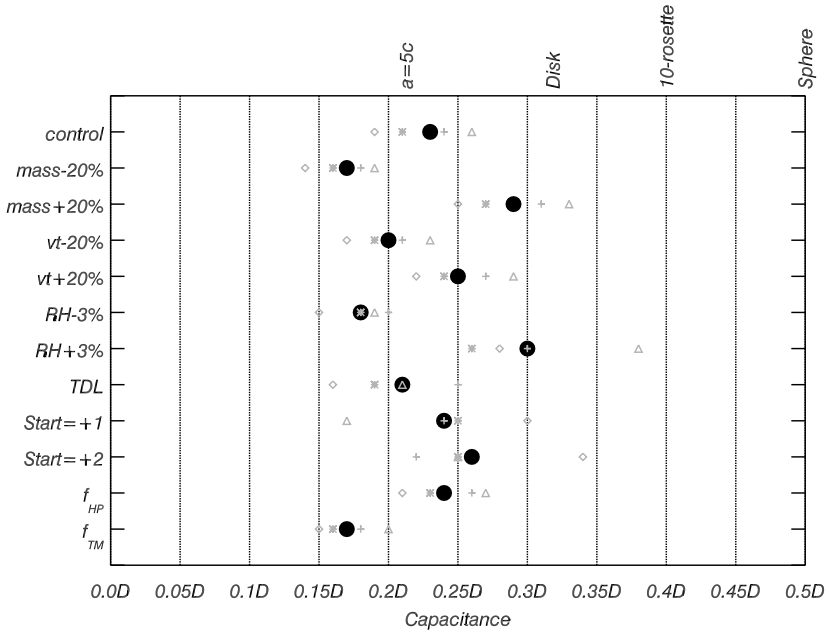

Figure 4: Results of a sensitivity test on the robustness of the capacitance determination. The solid circle represents the capacitance that provided the best match between the predicted IWC from all four regions simultaneously and the integrated PSD IWC. The grey symbols (see fig. 1) represent the capacitance that provided the best fit when each of the regions was considered separately. Each row represents the results from the control run, varying the mass dimension relation by $\pm$20%, varying the particle fallspeeds by $\pm$20%, varying the measured relative humidity by $\pm$3%, using the TDL derived relative humidity, lowering the start position for the analysis by 1 and 2 levels and introducing alternative relations for the ventilation coefficient (see text). Theoretical capacitance values are indicated along the top edge of the plot for a 5:1 column (a=5c), a disk, a 10 arm rosette (Chiruta and Wang 2003) and a sphere.

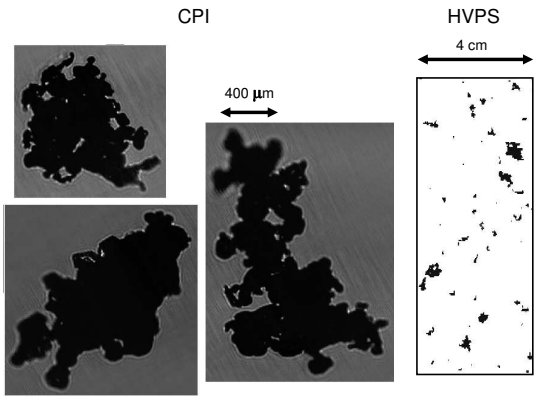

Figure 5: Example imagery from the CPI and HVPS probes obtained at 21:40 during the descent. The pixel size of the CPI is 2.5 μm while the HVPS has a pixel size of 200x400μm. The time lines have been omitted.

dard deviation in the IWC computed for each region. This approach leads to an estimated error of 7%. Both these potential errors are smaller than that carried out in the sensitivity tests for biases in the ice particle masses.

Examples of particles sampled during this descent (around 21:40) are shown in fig. 8 from the Cloud Particle Imager (CPI, pixel size: 2.5μm) and the HVPS (pixel size 200x400μm). While the CPI cannot image the large particles responsible for most of the change in IWC it can give an indication of the higher resolution structure of the larger ones imaged by the HVPS at lower resolution. The CPI images show $\sim$1 mm sized aggregates of individual $\sim$100μm crystals that appear rounded due to the effects of sublimation with many arms protruding from the periphery. The HVPS images show that the larger aggregate particles tend to be elongated and possess arms extending from the periphery.

Although the capacitance obtained for snowflakes is close to that expected for a 5:1 column, these particles in no way resemble such a simple geometry. The authors are not aware of any work that documents the capacitance of fractal particles, but any theoretical approach would probably follow Chiruta and Wang (2003) in assuming similarity with metallic conductors but using model aggregates (e.g. Westbrook et al. 2004).

Analysis of aircraft data suggest that a snowflake capacitance of 0.23D is able to reconcile the observed change in IWC with that predicted from observed parameters Further, sensitivity test show that this is a robust result. This value provides some justification for models that have made use of the capacitance of a disk to represent snow (0.32D) and indicates that those models that are assuming a spherical geometry are overestimating the sink of water vapor by a factor of $\sim$2.

Acknowledgements We gratefully acknowledge the hard work and dedication provided by the University of North Dakota's Citation aircrew, groundcrew, and support personnel.

6. REFERENCES

Bailey, M., Hallett, J. 2004: Growth rates and habits of ice crystals between-20 degrees and-70 degrees C. J. Atmos. Sci., 61 (5): 514-544.

Chiruta, M., Wang, P.K., 2003: The capacitance of rosette ice crystals J. Atmos. Sci., 60 (6): 836-846.

Chiruta, M, Wang, P.K., 2005: The capacitance of solid and hollow hexagonal ice columns geophysical research letters, 32 (5): art. no. l05803.

Field P.R., Heymsfield A.J. Bansemer A. 2006. A test of ice self collection kernels using aircraft data. J. Atmos. Sci., 63, 651-666.

Hall W. D., Pruppacher H.R., 1976: The survival of ice particles falling from cirrus clouds in subsaturated air. J. Atmos. Sci. 33, 1995-2006.

Ji, W.S., Wang, P.K., 1999: Ventilation coefficients for falling ice crystals in the atmosphere at low-intermediate Reynolds numbers. J. Atmos. Sci., 56 (6): 829-836.

McDonald J.E., 1963: Use of the electrostatic analogy in studies of ice crystal growth. Z. Angew. Math. Phys., 14, 610-619.

Podzimek, J., 1966: Experimental determination of the capacity. of ice crystals. Studia Geophys. Geodet., 10, 235238.

Pruppacher, H. R., Klett, D. J., 1997: Microphysics of clouds and precipitation. 954pp, Kluwer, Netherlands.

Pruppacher, H. R., Rasmussen, R. 1979: Wind-tunnel investigation of the rate of evaporation of

large water drops falling at terminal velocity in air. J. Atmos. Sci., 36 (7): 1255-1260.

Thorpe, A. D., and B. J. Mason, 1966: The evaporation of ice spheres and ice crystals. Br. J. Appl. Phys., 17, 541548.

Westbrook C.D., Ball R.C., Field P.R., et al., 2004: Universality in snowflake aggregation Geophys. Res. Letters 31 (15): Art. No. L15104.